N-Heterocyclic carbene-stabilized gold nanoparticles with tunable sizes

N. Bridonneau, L. Hippolyte, D. Mercier, D. Portehault, M. Desage-El Murr, P. Marcus, L. Fensterbank, C. Chaneac, F. Ribot

N-Heterocyclic carbene-stabilized gold nanoparticles with tunable sizes†

N. Bridonneau, [a] L. Hippolyte,[a,b] D. Mercier, [c] D. Portehault, [a] M. Desage-El Murr, [b] P. Marcus, [c] L. Fensterbank, *[b] C. Chanéac [a] and F. Ribot *[a]

Received 31st January 2018,
Accepted 10th April 2018
DOI: 10.1039/c8dt00416a

A simple and straightforward synthesis of N-heterocyclic carbene (NHC)-protected gold nanoparticles is derived from (benz)imidazolium-AuX_4 complexes and $NaBH_4$ only. The proposed method allows size tuning, from 3 to 6 nm, by adding (benz)imidazolium bromide. Changing the reducing agent to tBuNH$_2$BH$_3$ shifts the size range to *ca.* 6–12 nm. A one pot protocol is also reported from AuCl, (benz)imidazolium bromides and $NaBH_4$, thereby providing an even more straightforward way of producing NHC-capped gold nanoparticles. In addition, X-ray photoelectron spectroscopy (XPS) is used to unambiguously evidence, on the nanoparticles, the covalent bond formed between the NHC and the surface gold atoms.

1. Introduction

Gold nanoparticles exhibit remarkable behaviours due to their plasmonic properties and large surface-to-volume ratios. Accordingly, they find numerous applications in imaging, medicine, and catalysis.[1,2] Depending on the synthesis conditions and nature of the surface-capping ligands, precise control over morphology, colloidal stability and properties can be achieved.[3] Besides thiols, which are the most classical ligands, numerous other ones have also been shown to stabilize gold nanoparticles: amines,[3a] phosphines,[4] carboxylates,[5] imidazoles[6] and polymers including polysaccharides[7] (*e.g.* chitosan[8] and sucrose[9]).

Among the possible capping ligands, N-heterocyclic carbenes (NHCs) are a current hotspot.[10] They form particularly strong bonds with various metals, the strength of which has been measured *ca.* 155 kJ mol^{-1} for self-assembled monolayers (SAMs) on gold and copper.[10f–g] This strong covalent bond with metals makes NHCs good candidates to obtain gold nanoparticles of small sizes and high colloidal stabilities.[11–14] Moreover, it might also allow a higher modulation of the nanoparticle properties by the organic moieties through an easier crosstalk between the ligand and the metallic core. Among the potential advantages of NHC-stabilized gold nanoparticles, improved catalytic properties for the electroreduction of CO_2 to CO and a high colloidal stability in biologically relevant media have already been documented.[11e,12e–f] Bidentate NHC ligands were also reported to yield ultrastable gold nanoparticles.[12g]

NHCs can be easily synthesized on a gram scale and their synthetic flexibility makes them promising ligands for targeting specific properties. Organometallic chemistry,[15] catalysis,[16] design of metallodrugs,[17] and functional coatings are currently explored using NHCs.[10,18]

Four main synthetic strategies have been used so far to prepare NHC-coated gold nanoparticles. The first one, originally described by Hurst *et al.*,[11a] relies on ligand exchange on nanoparticles previously synthesized with a sacrificial labile ligand such as didodecylsulfide or oleylamine.[11] The second strategy, first proposed by Vignolle *et al.*,[12a] involves the reduction of Au(I) molecular species already having an NHC bound to the metallic center, [(NHC)AuX] (X = Cl or Br) or [Au(NHC)$_2$](O$_3$SCF$_3$).[12] The third one, described by Serpell *et al.*,[13a] starts with (benz)imidazolium haloaurate salts, [(Benz)Imid](AuX$_4$), which are first treated with NaH, a strong base, to generate the NHC, and then reduced with $NaBH_4$.[13] Finally, ultrasmall NHC-coated gold nanoparticles, with a size below 1.5 nm, have been obtained by the solvent free thermolysis of [Imid][Au(C$_6$F$_5$)$_2$] or [Au(C$_6$F$_5$)(NHC)].[14]

Size tuning for gold nanoparticles has been reported for many different capping agents, but except for the very recent work by Salorinne *et al.*,[12f] in which NHC-stabilized gold nano-

[a]*Sorbonne Université, CNRS, Collège de France, Laboratoire de Chimie de la Matière Condensée de Paris, LCMCP, F-75005 Paris, France.*
E-mail: francois.ribot@sorbonne-universite.fr
[b]*Sorbonne Université, CNRS, Institut Parisien de Chimie Moléculaire, IPCM, F-75005 Paris, France. E-mail: louis.fensterbank@sorbonne-universite.fr*
[c]*PSL Research University, Chimie Paris Tech, CNRS, Institut de Recherche de Chimie Paris, IRCP, F-75005 Paris, France*

†Electronic supplementary information (ESI) available: X-ray crystal structure determinations (Table S1 and Fig. S1–S3); TEM images, size distributions and UV-Vis spectra for various syntheses (Fig. S5 and S6); FT-IR (Fig. S7); mass spectrometry (Fig. S8); XPS (Fig. S9 and S10); TEM images and size distributions for syntheses from AuCl (Fig. S11); ^{1}H and ^{13}C NMR spectra for (benz)imidazolium bromide and haloaurate. CCDC 1548811 and 1548812. For ESI and crystallographic data in CIF or other electronic format see DOI: 10.1039/c8dt00416a

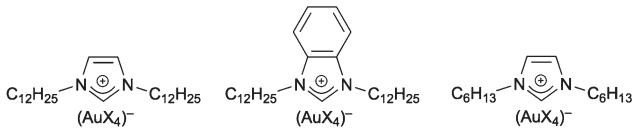

1-AuX$_4$ **2-AuX$_4$** **3-AuX$_4$**

Scheme 1 (Benz)imidazolium-AuX$_4$ complexes used as precursors of the synthesis of gold nanoparticles.

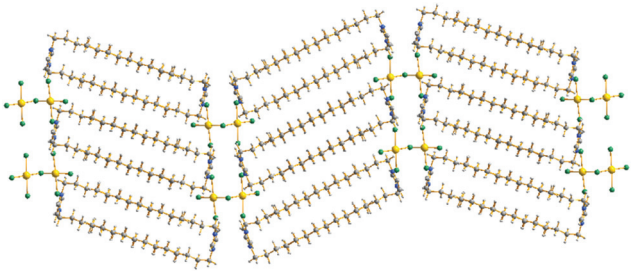

Fig. 1 Molecular structure of **1-AuX$_4$** complex (color code: Au = yellow, Cl/Br = green, N = blue, C = grey, H = light grey).

particles with tunable core diameters between 2.0 and 3.3 nm were obtained by varying the reaction time, none of the previously reported syntheses have described an extended modulation of the size for the NHC-coated gold nanoparticles.

Herein, we report a methodology that revisits and extends Serpell's seminal synthesis from (benz)imidazolium haloaurate salts.[13a] First, it bypasses the low temperature NaH-based deprotonation step and directly proceeds with the reduction by $NaBH_4$, making the process easier. Then, we show that the nanoparticle size can be tuned by adding extra (benz)imidazolium halide. Despite the absence of NaH, the formation of NHCs and their bonding to the nanoparticle surface is evidenced, in particular by X-ray photoelectron spectroscopy (XPS). We also show that replacing sodium borohydride by *tert*-butylamine borane shifts the tuning range towards larger sizes. Finally, we introduce an even simpler protocol, in which $NaBH_4$ reacts with AuCl in the presence of (benz)imidazolium bromide.

2. Results and discussion

2.1. Synthesis and characterization of (benz)imidazolium haloaurate salts

Three (benz)imidazolium haloaurate salts, with lateral chains from C6 to C12 to allow steric stabilization (Scheme 1), were prepared according to the reported procedures,[19] from imidazole (or benzimidazole). X-Ray quality crystals of **1-AuX$_4$** and **2-AuX$_4$** were obtained by the slow diffusion of EtOH into a $CHCl_3$ solution of the complexes, while complex **3-AuX$_4$** was recovered as an orange oil.

Both **1-AuX$_4$** and **2-AuX$_4$** compounds crystallize in the monoclinic system ($P2_1/c$ and $P2_1/n$ space groups, respectively)‡ as alternating layers of anions and cations (Fig. 1 and S1–S3, Table S1†). This particular arrangement, which has already been reported in the literature, is likely driven by the packing of the long alkyl chains.[13a]

For both compounds, the anionic layer shows the presence of a mixed species with the replacement of approx. one-fourth of chlorine atoms by bromine atoms, giving the resulting composition: $AuCl_{4-x}Br_x$ (with $x \sim 1$). The bromine atoms originate from the last synthetic step that consists of **1-Br** reacting with $HAuCl_4{\cdot}3H_2O$. In the following structural description, the anions will be referred to as AuX_4^- (X = Cl or Br), with mean atomic distances between those of Br and Cl.

Within the anionic layer, AuX_4^- units show a square planar geometry, with an average Au–X distance of 2.33 Å. They are roughly arranged perpendicularly to one another, with dihedral angles of 88.45(1)° for **1-AuX$_4$** and 85.14(3)° for **2-AuX$_4$**. Anions are well separated from each other, with Au–Au shortest distances of 5.7710(2) Å for **1-AuX$_4$** and 6.1637(1) Å for **2-AuX$_4$**, which precludes aurophilic interactions.[20]

Yet, infinite $[AuX_4]_n$ chains can also be considered with corner to face contacts, as in the previously reported compounds,[13a,21] corresponding to an interionic Au···X distance of 3.494(1) and 3.859(1) for **1-AuX$_4$** and **2-AuX$_4$**, respectively. For **1-AuX$_4$**, the closest contact between anions and cations corresponds to a C–H···X interaction that involves the imidazolium-bound proton (H2···X4 = 2.6664 Å) and is associated with a C2···X4 distance of 3.5489(1) Å. The halogen atom involved in this contact is located in the imidazolium plane. Instead, for **2-AuX$_4$** the closest interaction involves a hydrogen of the benzene ring (H6···X2 = 2.7804 Å) with a C6···X2 distance of 3.4784(1) Å.

In both structures, ligands **1** and **2** are arranged in a head-to-tail manner and exhibit hydrophobic interactions among the aliphatic chains of two adjacent molecules, the shortest intermolecular C···C contact being 3.925(8) Å for **1-AuX$_4$** and 3.63(1) Å for **2-AuX$_4$**. Such hydrophobic interactions are likely the driving force of crystallization.

2.2. Is the use of NaH mandatory?

In their report on NHC-coated gold nanoparticle synthesized from **3-AuCl$_4$**, Serpell *et al.* have concluded that the addition of NaH was necessary.[13a] This point was never questioned in the subsequent studies that used the same protocol.[13b,c] However, strong bases, such as NaH, being delicate to introduce in a

‡Crystal data for **1-AuCl$_3$Br**: Orange plate-like crystals, $C_{27}H_{53}AuBrCl_3N_2$, monoclinic, $P2_1/c$, a = 8.4845(4), b = 42.119(2), c = 9.4482(5) Å, β = 102.912(2)°, V = 3291.0(3) Å^3, Z = 4, T = 200(2) K, μ = 5.950 mm^{-1}, 27 789 reflections measured, 5785 independent (R_{int} = 0.0226), 5469 observed [$I \geq 2\sigma(I)$], 309 parameters, final R indices R_1 [$I \geq 2\sigma(I)$] = 0.0264 and wR_2 (all data) = 0.0574. CCDC 1548811. Crystal data for **2-AuCl$_3$Br**: Orange block-like crystals, $C_{31}H_{55}AuBrCl_3N_2$, monoclinic, $P2_1/n$, a = 9.1187(2), b = 10.1455(3), c = 39.2531(10) Å, β = 90.2110(10)°, V = 3631.43(16) Å^3, Z = 4, T = 200(2) K, μ = 5.330 mm^{-1}, 104 767 reflections measured, 10 687 independent (R_{int} = 0.0493), 8429 observed [$I \geq 2\sigma(I)$], 349 parameters, final R indices R_1 [$I \geq 2\sigma(I)$] = 0.0680 and wR_2 (all data) = 0.1251. CCDC 1548812.

clean and reproducible way, the possibility to avoid their use was explored.

2.2.1. NaH free protocol with 1-AuX$_4$. The imidazolium haloaurate salt was first dissolved in toluene, dichloromethane or a mixture of both, yielding orange solutions. A fresh aqueous solution of $NaBH_4$ was then added dropwise, causing an instant color change from orange to deep red. The biphasic mixture was allowed to react for approx. 10 min before washing the organic solution with water. The suspended gold nanoparticles were finally precipitated with ethanol. Following this protocol with **1-AuX$_4$** yields round-shaped gold nanoparticles of 5.8 ± 1.0 nm as evidenced by transmission electron microscopy (TEM) (Fig. 2a).

As the ligand-to-gold ratio is known to have an impact on the nanoparticle size,[5] we then investigated the effect of **1-Br** addition on the resulting size. Four equivalents of imidazolium bromide, with respect to gold, were added to the initial haloaurate salt, causing a slight color change from light orange, without **1-Br**, to red. Then a fresh aqueous solution of $NaBH_4$ was added to produce particles with a mean diameter of 4.0 ± 0.9 nm (Fig. 2b). Hence, increasing the amount of NHC precursors decreases the particle size, in agreement with the usual behaviour observed for various surface stabilizing ligands, *e.g.* thiols and citrates.[22] However, a further increase of the **1-Br**/Au ratio, up to 10, did not yield any additional change in the particle size. These nanoparticles exhibit a localized surface plasmon band at 524 nm (in dichloromethane) when only **1-AuX$_4$** is used, and at 519 nm when the synthesis is carried out with **1-AuX$_4$** and 4 equivalents of **1-Br**. This evolution of λ_{max} with the particle size follows the usual hypsochromic shift.[23]

2.2.2. NaH free *vs.* NaH containing protocol for 1-AuX$_4$. In order to compare our NaH-free protocol with those in the literature,[13] we also carried out experiments with NaH. In such cases, the addition of NaH to the imidazolium-AuX_4 solution (NaH/Imid ~1.5) was performed at 0 °C in toluene or a toluene/dichloromethane mixture. It caused discoloration of the solution within 10 to 20 minutes. Afterwards, a fresh aqueous solution of $NaBH_4$ was added to reduce Au(III) and generate metallic nanoparticles. Experiments were carried out in the absence or presence of extra **1-Br**. In both cases (Table 1 and Fig. S4†), the nanoparticles exhibit similar size distributions but are smaller by approx. 1 nm when NaH is used. These observations suggest that the presence of NaH impacts nucleation/growth mechanisms: NaH could indeed favor imidazolium deprotonation and increase the amount of NHC generated, thus providing more ligands to stabilize smaller particles with a larger surface-to-volume ratio.

All in all, gold nanoparticles with sizes ranging from 3.3 ± 0.9 to 5.8 ± 1.0 nm can be obtained from the same bis(*N*,*N*′-dodecyl)imidazolium haloaurate by simply introducing NaH or not and adding extra imidazolium bromide or not.

2.2.3 Influence of the ligands. To assess the generality of our NaH free synthesis, we have investigated two other precursors: **2-AuX$_4$** and **3-AuX$_4$** (Table 1 and Fig. S5 and S6†). For **2-AuX$_4$**, a benzimidazolium based compound, the particles are smaller when extra NHC precursors are used, as previously observed for **1-AuX$_4$**. However, for **2-AuX$_4$**, the gold nanoparticle sizes are smaller than those observed for **1-AuX$_4$**. Moreover, for **2-AuX$_4$**, the absence or presence of NaH impacts the size more moderately than that for **1-AuX$_4$**. These results are likely related to an easier formation of NHCs from benzimidazolium than from imidazolium.[24] **3-AuX$_4$**, which bears two shorter lateral chains (*n*-hexyl *vs.* *n*-dodecyl), behaves quite differently from **1-AuX$_4$** and **2-AuX$_4$**. Indeed, it does not yield stable nanoparticles when no NaH is added, as previously reported.[13a] However, when 4 equivalents of **3-Br** are added to **3-AuX$_4$**, stable nanoparticles can be obtained without NaH. Finally, with a starting mixture enriched in **3-Br** and the addition of NaH prior to $NaBH_4$, the obtained particles are only moderately smaller than those with the NaH free protocol.

Thus the NaH free protocol does not appear to be efficient with the *n*-hexyl derivative, which presents a lower stabilizing

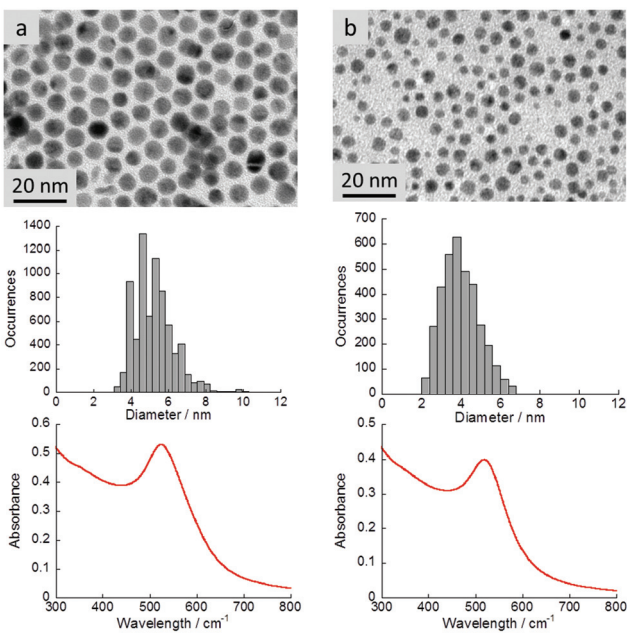

Fig. 2 TEM images, size distributions and UV spectra of the corresponding suspension in dichloromethane for gold nanoparticles obtained in NaH free syntheses with (a) only **1-AuX$_4$** (size = 5.8 ± 1.0 nm and λ_{max} = 524 nm) or (b) a mixture of **1-AuX$_4$** and 4 equivalents of **1-Br** (size = 4.0 ± 0.9 nm and λ_{max} = 519 nm).

Table 1 Average particle sizes (nm) as measured by TEM, for nanoparticles obtained without or with NaH and without or with 4 equivalents of (benz)imidazolium bromide

Precursors	$NaBH_4$ only	NaH and $NaBH_4$
1-AuX$_4$	5.8 ± 1.0	4.8 ± 1.1
1-AuX$_4$ + 4 **1-Br**	4.0 ± 0.9	3.3 ± 0.9
2-AuX$_4$	4.9 ± 1.1	4.4 ± 1.2
2-AuX$_4$ + 4 **2-Br**	3.6 ± 0.8	3.9 ± 0.7
3-AuX$_4$	Not stable	3.2 ± 0.8
3-AuX$_4$ + 4 **3-Br**	4.1 ± 1.0	3.6 ± 0.6

effect, but it is fully operational with (benz)imidazolium compounds bearing longer lateral chains (*i.e.* dodecyl). All these observations show that the nanoparticle synthesis is not only driven by the presence or absence of NaH but also by the (benz)imidazolium/Au ratio, which probably modulates the amount of generated carbenes.

2.3. Nature of the capping ligands and their interaction with gold nanoparticles

Our simplified protocol raises the question regarding the exact nature of the capping ligands on the so-obtained gold nanoparticles. Indeed, as NaH was originally used to deprotonate the imidazolium and generate the NHC,[13a] its absence might result in nanoparticles stabilized by imidazoliums that interact electrostatically with the surface and not by carbenes attached through C–Au bonds. Actually, the answer to this question is not obvious as there are only a few reported pieces of evidence, mainly by ^{13}C solid state NMR, for the formation of C–M bonds in NHC-protected metal nanoparticles.[11b,f,14,25]

To check for the presence of imidazolium, ^{1}H NMR was performed on concentrated toluene-d_8 suspensions of purified gold nanoparticles prepared from **1-AuX$_4$**. No signal related to the imidazolium proton was detected in the region from 8 to 13 ppm, but the two other protons of the heterocycle as well as the N–CH_2 protons (~4.5 ppm) were also not observed. Only the terminal methyl groups (*ca.* 0.9 ppm) and the main chain methylene groups (*ca.* 1.2 ppm) were seen. This disappearance of the signals associated with sites near the surface of nanoparticles, which can arise from the surface heterogeneities and the slow tumbling of the particles that shortens the transverse relaxation rate, has already been reported.[12a,14,25a] If it indicates that the heterocycle is close to the surface, it does not allow us to conclude its nature: imidazolium or carbene.

Comparison of the FTIR spectra of the precursors and gold nanoparticles (Fig. 3 and S7†) reveals some modifications. The spectra of **1-Br** and **1-AuX$_4$** are similar, except for slight modifications of two bands (shifts from 1636 to 1616 cm^{-1} and 773 to 757 cm^{-1}). They are in agreement with the reported data and calculations on similar systems.[26] In contrast, gold nanoparticles exhibit a strongly modified spectrum, with a new band at 1410 cm^{-1} and the disappearance of two bands at 1616 and 1563 cm^{-1}, which are located in the region of the ν(C=N) and ν(C=C) stretching vibrations of the imidazolium aromatic ring. These latter modifications strongly suggest the formation of NHCs and their coordination on the gold surface.[12e] It is worth mentioning that the ν(C–H) stretching vibration, near 3270 cm^{-1}, associated with the imidazolium proton, is not observed for any of the three samples, possibly because of its expected very low intensity.

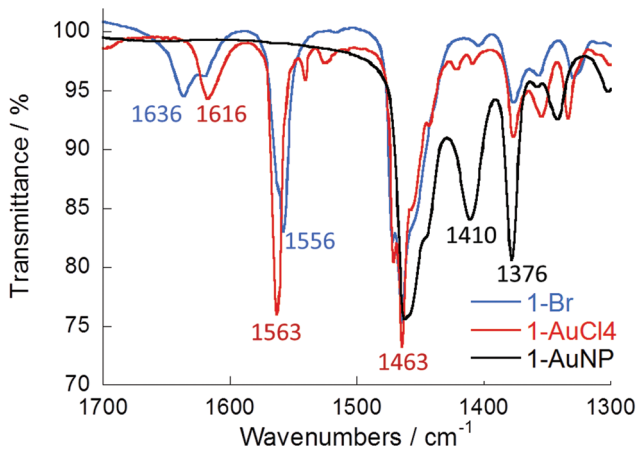

Fig. 3 IR spectra of **1-Br** (blue trace), **1-AuX$_4$** (red trace) and gold nanoparticles prepared from **1-AuX$_4$** (black trace).

An additional clue for the deprotonation of the imidazolium and the formation of a covalent Au–C bond was given by mass spectrometry. Indeed, the ethanol supernatant of a typical synthesis (such as the reaction of **1-AuX$_4$** and $NaBH_4$) contains the molecular complex $[Au(NHC)_2]^+$ (m/z = 1005.79 for the NHC derived from **1**, Fig. S8†) that could be one of the first intermediates towards the formation of gold nanoparticles.[14]

Finally, X-ray photoelectron spectroscopy (XPS) was used to get a better insight into the carbon–gold interaction. This technique enables the user to determine the chemical state of an analyzed surface, and, at the same time, can provide a very accurate elemental composition. Thus it is commonly used for surface characterization in many areas (sensor, corrosion, and catalysis). For nanoparticle characterization, XPS seems very promising as it can be used to assess the integrity of the stabilizing agent on the nanoparticle surface. More interestingly, XPS can be used to gather information about the capping mode of the ligand on the metallic surface. However, using XPS on nanoparticles is still very challenging, for multiple reasons (peak widening, need to deposit the particles on a conductive surface, *etc.*).

XPS has already been used for NHC-coated palladium,[27] platinum[28] and gold nanoparticles.[12f–h] The presence of the capping ligand was evidenced with the C 1s and N 1s photopeaks, the position of the latter being used to confirm the binding of the NHCs.[12f–h] However, none of these studies have reported an XPS derived elemental composition of the ligands, hence showing the difficulties of a thorough characterization of the nanoparticles by XPS. Moreover, no clear XPS evidence of a covalent carbon–metal bond was presented.

XPS analyses were carried out on two samples: **1-Br** and gold nanoparticles prepared from **1-AuX$_4$** mixed with 4 equivalents of **1-Br** (**1-AuNP**). Each photopeak has been carefully deconvoluted to assess the possible presence of several components. Results are reported in Table 2. For **1-Br**, its Br 3d photopeak can be split into Br $3d_{5/2}$ and Br $3d_{3/2}$ at 67.4 and 68.3 eV, respectively (Fig. S9†). For **1-AuNP**, the absence of a peak in the 185–210 eV and 65–72 eV regions indicates that the sample contains neither chlorine nor bromine, confirming the correct purification of gold nanoparticles and the absence of any cationic species that would require counter anions.

For **1-AuNP**, the formation of metallic gold is clearly evidenced by its XPS Au 4f signal, which is composed of only two peaks at 84.0 and 87.6 eV in agreement with the spin–orbit

Table 2 XPS data (binding energy: BE, assignment and composition) for **1-Br** and **1-AuNP**

Sample /peak	BE [eV]	Assignment	Composition[a] [at%]	Calculated stoichiometry	Expected stoichiometry
1-Br/C 1s	285.0	Aliph. C	72.5	21.7	22
1-Br/C 1s	286.0	Aliph. C–N	7.2	2.2	2
1-Br/C 1s	286.5	N–HC═CH–N	7.3	2.2	2
1-Br/C 1s	287.2	N_2–C–H	3.6	1.1	1
1-Br/N 1s	401.6		6.1	1.8	2
1-Br/Br $3d_{5/2}$	67.4		3.3	1.0	1
1-AuNP/C 1s	285.0	Aliph. C	75.7	21.9	22
1-AuNP/C 1s	286.0	Aliph. C–N	6.9	2.0	2
1-AuNP/C 1s	286.4	N–HC═CH–N	6.9	2.0	2
1-AuNP/C 1s	284.1	N_2–C–Au	3.4	1.0	1
1-AuNP/N 1s	400.2		7.1	2.1	2
1-AuNP/Au 4f	84–90				

[a] Extracted from the fit.

coupling (Au $4f_{7/2}$ and Au $4f_{5/2}$, respectively). The energy shift between both components, 3.6 eV, is characteristic of Au(0). A very weak asymmetry can be observed on the high-energy side (Fig. S10†) as always for gold metallic surfaces. However, the absence of any additional contributions (Au(I), electrostatic, *etc.*) was confirmed by the very good fit of the Au 4f signal of **1-AuNP** using the parameters obtained from the analysis of a planar gold surface (Fig. S10†).

The N 1s photopeak of **1-Br** (Fig. 4) is symmetric and shows a unique component centered at 401.6 eV, as expected for this type of molecular environment. For **1-AuNP**, the N 1s spectrum also presents a single component (Fig. 4), but with a strong shift towards the weaker binding energy (Table 2). Such a shift has already been observed in the case of metallic nanoparticles stabilized by NHCs.[12f,27,28] This shifted contribution corresponds to a charge loss on the heterocycle, arising from the conversion of imidazolium into an NHC and its covalent binding to the gold surface. It has to be noted that the high signal to noise ratio for the N 1s peak of **1-AuNP** rules out the presence of any additional component. Accordingly, the NHC is the only species present on the nanoparticle surface. This well-defined peak also makes our results directly comparable to those obtained on flat gold substrates.[10d,29]

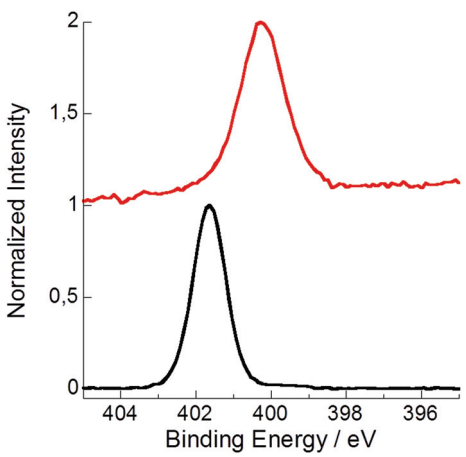

Fig. 4 N 1s XPS spectra for the imidazolium bromide **1-Br** (bottom trace) and gold nanoparticles **1-AuNP** (top trace).

To be fitted, the C 1s photopeak of **1-Br** requires four contributions, all with the same FWHM (Fig. 5a). Each of these contributions is characteristic of a given chemical environment: at 285.0 and 286.0 eV are found the aliphatic carbons (C–C and C–N, respectively), while at 286.5 and 287.2 eV appear the carbons of the aromatic heterocycle (C–C–N and N_2–C–H, respectively).[30] Importantly, the stoichiometric coefficients derived from this fit match very well with those expected from the formula of **1-Br** (Table 2). The overall composition in carbon, nitrogen and bromine also agrees very well.

For **1-AuNP**, the C 1s spectrum was fitted with five components (Fig. 5b). Components 1, 2 and 3 correspond to those found for **1-Br** and are attributed to C–C aliphatic, C–N aliphatic and C–C–N aromatic environments. A fourth contribution was found at 284.1 eV. It can be assigned to a N_2–C–Au environment. Such a contribution has already been observed on gold and iron flat substrates.[31,32] Moreover, the absence of the N_2–C–H contribution, which appeared on the high binding energy side at 287.2 eV for **1-Br**, confirms the carbene formation and the absence of imidazolium on the nanoparticle surface. The relative intensities of these four components agree very well with the atomic compositions of the capping ligand (Table 2), as does the overall composition in carbon and nitrogen. It is worth mentioning that the absence of boron, which could originate from the reducing agent, was also checked by XPS, hence ruling out the possibility of an N_2–C–B environment.

The fifth C 1s component, located at high binding energy (288.50 eV) can be attributed to the $\pi \rightarrow \pi^*$ transition, which is characteristic of a shake-up peak (satellite peak) originating from the photoelectron excitation of the heterocycle ring.[33] In the present case, this satellite peak is only observed for **1-AuNP**, which suggests an enhancement by the plasmonic effect (plasmon loss satellite).

In conclusion, XPS allows us to conclude that the reported NaH free protocol yields gold nanoparticles coated with NHCs. Actually, $NaBH_4$, which is added in excess (10 eq. relatively to

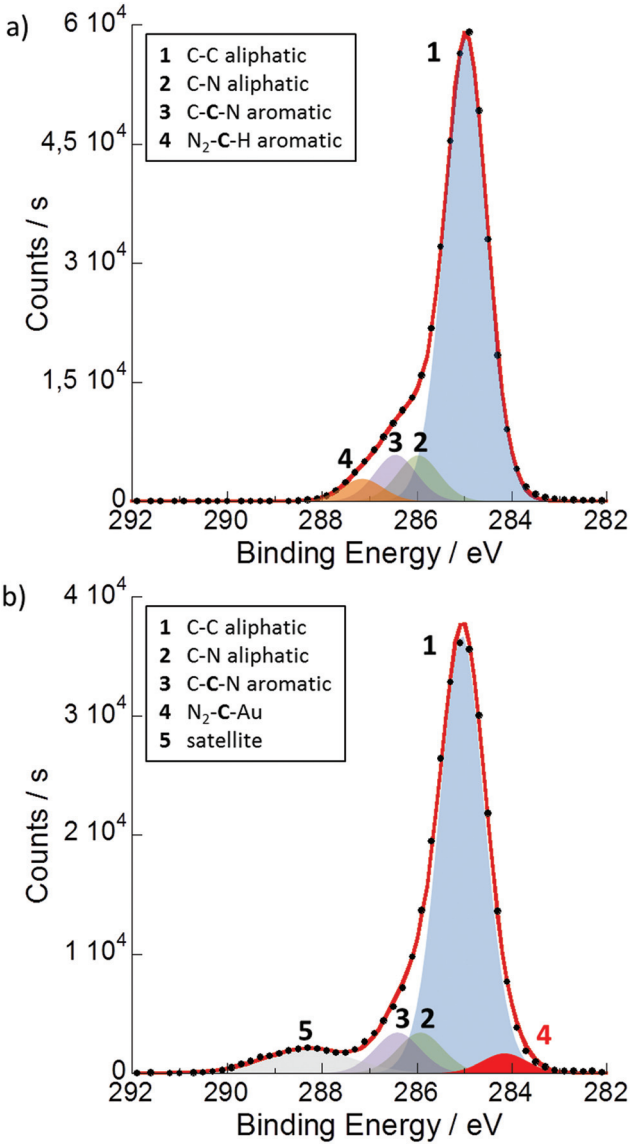

Fig. 5 C 1s XPS spectra and their corresponding fits for (a) the imidazolium precursor **1-Br** and (b) gold nanoparticles **1-AuNP**.

Au) may be basic enough to deprotonate the (benz)imidazolium, as already suggested in the literature.[34] Finally, to the best of our knowledge, the present work is the first report of the C 1s XPS signal associated with N_2–C–Au environments on the surface of a gold nanoparticle.

2.4. Changing $NaBH_4$ for *tert*-butylamine borane

We then investigated the NaH free protocol with a milder reducing agent: tBuNH$_2$BH$_3$. Such a reagent also has the advantage of being soluble in toluene, thus allowing a single-phase synthesis, which usually yields narrower size distribution.[35] Using **1-AuX$_4$** as a precursor, the influence of the reaction time (from 2 min to 3 h) and of the temperature (from 0 °C to 110 °C) was investigated. Large spheroidal nanoparticles (20–25 nm in diameter), mixed with some rods (80 × 20 nm), were obtained and tend to coalesce when increasing either the reaction time or the temperature. Surprisingly, experiments carried out with the addition of NaH produced drastically different outcomes. Indeed, adding NaH prior to the reduction with tBuNH$_2$BH$_3$, does not yield any nanoparticles but leads to bulk materials, suggesting that the deprotonation step is not the only issue at stake for the nucleation/growth mechanism.

The effect of the ligand/gold ratio was also investigated with tBuNH$_2$BH$_3$. Fig. 6 shows the TEM images and size distributions of the nanoparticles obtained with different **1-AuX$_4$: 1-Br** ratios, varying from 1 : 0 (**1-AuX$_4$** only) to 1 : 6. All experiments were carried out at 55 °C with 10 min of stirring. The as-obtained nanoparticle size and shape dramatically depend on the addition of **1-Br**. The particles change from large and polydisperse (24 ± 7 nm), with ill-defined shapes and a few rods, when only **1-AuX$_4$** is used (ratio 1 : 0), to smaller and round shaped with a more homogeneous size distribution when increasing the amount of **1-Br**. At least 1 equivalent of **1-Br** seems to be necessary to obtain a reasonable size distribution (~25%). For 6 equivalents of **1-Br**, the nanoparticles reach a size of 5.8 ± 1.1 nm. Accordingly, when tBuNH$_2$BH$_3$ is used as a reducing agent, the ligand/gold ratio appears as a

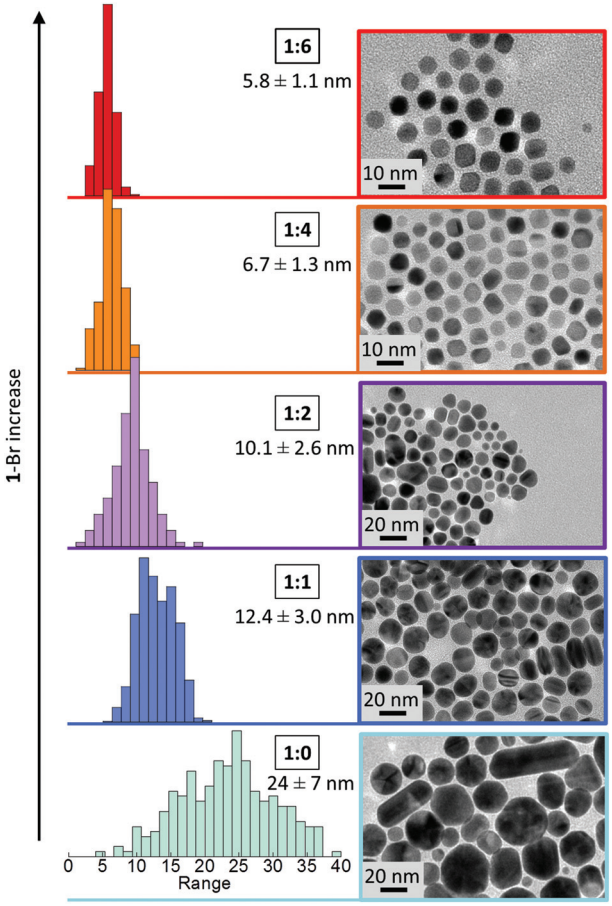

Fig. 6 TEM images and corresponding size distributions of gold nanoparticles obtained from **1-AuX$_4$** and various amounts of **1-Br** (from 0 to 6 eq.) with tBuNH$_2$BH$_3$ as a reducing agent (10 min stirring at 55 °C in toluene).

possible leverage towards the control of the particle size over the range 6 to 12 nm.

The localized surface plasmon band of these gold nanoparticles changes only moderately with their size: from 530 nm for nanoparticles of 10–12 nm, to 525 nm for nanoparticles around 6 nm.

2.5. Towards a simpler gold source

As the synthesis of NHC-protected gold nanoparticles does not require NaH to deprotonate the imidazolium, and adding imidazolium bromide can tune the size, we decided to take a step further and explore the synthesis of gold nanoparticles following an even simpler synthetic pathway: the direct reduction of AuCl by $NaBH_4$ in the presence of imidazolium bromide. The addition of **1-Br** to AuCl dissolved in toluene causes a color change from colorless to orange, reflecting an interaction of the reactants, which is also evidenced by the NMR shift of the imidazolium proton. The subsequent addition of $NaBH_4$ immediately produces visible gas evolution, likely forming H_2 as a by-product of the reduction of Au(I) as well as of the deprotonation of the imidazolium. The obtained nanoparticles exhibit isotropic shapes (Fig. 7a). Experiments carried out with the **2-Br** or **3-Br** precursor showed similar sizes: 4.4 ± 0.8 nm (Fig. 7b) and 3.7 ± 0.8 nm (Fig. S11†), respectively. Finally we noted that if NaH is added to the mixture of AuCl and **1-Br** before $NaBH_4$, the nanoparticles obtained are slightly bigger (4.3 ± 0.9 nm, Fig. S11†) than those without NaH (3.7 ± 0.9 nm), contrary to what was observed with **1-AuX$_4$**. Finally, in this synthesis with AuCl and (benz)imidazolium bromide, varying the ligand/gold ratio, up to 6, did not influence the particle size.

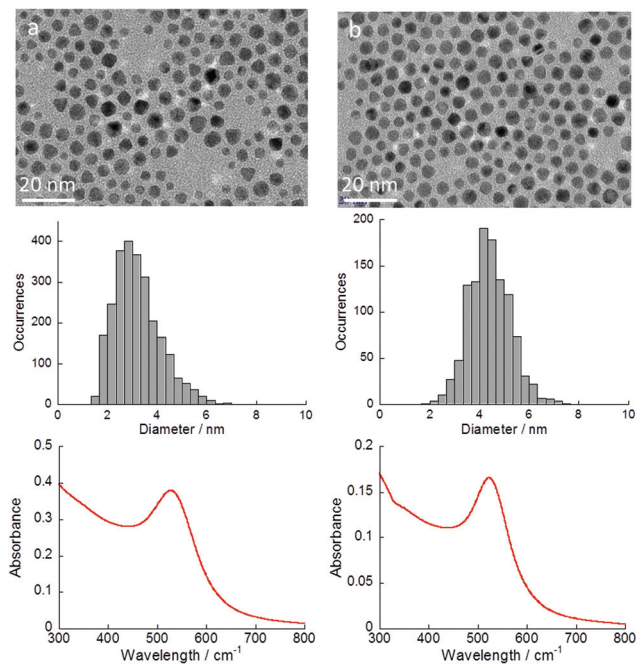

Fig. 7 TEM images, size distributions and UV spectra of gold nanoparticles obtained from AuCl and (a) **1-Br** (size = 3.7 ± 0.9 nm and λ_{max} = 527 nm) or (b) **2-Br** (size = 4.4 ± 0.8 nm and λ_{max} = 523 nm).

It is worth noting that, while the examples of NHC protected gold nanoparticles were already reported from Au(I) precursors, the related protocols always involved the isolation of [Au(NHC)X] complexes.[12] Accordingly, our protocol is the first to provide stable gold nanoparticles directly from AuCl and readily available (benz)imidazolium halides.

Compared to the synthesis starting from (benz)imidazolium haloaurate, this synthesis with AuCl and (benz)imidazolium halide likely follows an other chemical pathway as the effects observed upon adding NaH before $NaBH_4$ or extra (benz)imidazolium halide are different. The various oxidation degrees of the precursors likely modify the intermediate complexes that might be involved as well as the reduction and nanoparticle formation process. For instance, Jin *et al.* have shown that,[22b] in Turkevich's synthesis,[5] pH changes modify the reaction pathway through the structure of the reactants involved.

3. Conclusion

Straightforward syntheses of NHC-protected gold nanoparticles have been presented from (benz)imidazolium-AuX_4 precursors. Compared to previous studies,[13] our protocols do not require the addition of NaH. Yet, the *in situ* generation of carbenes has been confirmed, in particular by X-ray photoelectron spectroscopy, which has evidenced C–Au bonds on the surface of nanoparticles. Particle size tuning was obtained *via* the addition of (benz)imidazolium bromide. With $NaBH_4$, sizes from 6 to 4 nm, or even 3 nm when NaH is also added, can be obtained. However, the tuning range depends on the (benz)imidazolium used. With precursors **1-AuX$_4$** and *t*$BuNH_2BH_3$, instead of $NaBH_4$, the particle size can be modified from 12 to 6 nm. Finally, stable gold nanoparticles around 4 nm have also been obtained very simply by reducing AuCl with $NaBH_4$ in the presence of (benz)imidazolium bromide. All in all, the possibility offered by these syntheses opens the way to the development of hybrid nanoparticles of tuned sizes with functionality derived from N-heterocyclic carbenes strongly anchored on the gold surface.

4. Experimental methods

4.1. Syntheses

4.1.1 Chemicals. $HAuCl_4{\cdot}3H_2O$, $NaBH_4$, NaH (60% in oil), *t*$BuNH_2BH_3$, imidazole, benzimidazole, *n*-dodecyl bromide and *n*-hexyl bromide have been purchased from Sigma Aldrich or Fluka and used as received. Solvents were purified by classical techniques and water was purified through a Milli-Q system.

4.1.2 Syntheses of (benz)imidazolium bromides. Compounds were prepared in two steps from imidazole (or benzimidazole) and the corresponding alkyl bromide, in the

presence of NaH, following a procedure reported for **3-Br**.[19] The procedure was adapted for **1-Br** and **2-Br**. After refluxing the reactants in THF, the mixture was evaporated under reduced pressure. The residue was dissolved in dichloromethane and filtered, then the solvent was evaporated again and the new residue was dissolved in diethyl ether and left at 4 °C for 2 h. After filtration, the precipitate was dried under vacuum to give the product as a white powder.

1-Br (yield 77%). ^{1}H NMR (400 MHz, $CDCl_3$) δ 10.88 (1H, s, NC*H*N), 7.20 (2H, d, NC*HCH*N), 4.36 (4H, t, $NCH_2C_{11}H_{23}$), 1.92 (4H, q, $NCH_2CH_2C_{10}H_{21}$), 1.35–1.25 (36H, m, $N(CH_2)_2C_9H_{18}CH_3$), 0.88 (6H, t, $N(CH_2)_{11}CH_3$); ^{13}C NMR (101 MHz, $CDCl_3$) δ 137.70 (NH*C*N), 121.78 (NH*CC*HN), 50.29 (NCH_2), 32.00, 30.44, 29.70, 29.60, 29.49, 29.43, 29.11, 26.37, 22.78, 14.22 (CH_3); HRMS calculated for $C_{27}H_{53}N_2^+$, *m*/*z*: 405.4203, found: 405.4197.

2-Br (yield 78%). ^{1}H NMR (400 MHz, $CDCl_3$) δ 11.57 (1H, s, NC*H*N), 7.67 (4H, m, C_6H_4), 4.62 (4H, t, $NCH_2C_{11}H_{23}$), 2.06 (4H, q, $NCH_2CH_2C_{10}H_{21}$), 1.44–1.24 (36H, m, $N(CH_2)_2C_9H_{18}CH_3$), 0.87 (6H, t, $N(CH_2)_{11}CH_3$); ^{13}C NMR (75 MHz, $CDCl_3$) δ 142.93 (N*H*CN), 131.44, 127.18, 113.19, 47.79 (NCH_2), 31.98, 29.67, 29.58, 29.47, 29.40, 29.14, 26.65, 22.76, 14.20 (CH_3).

3-Br (yield 60%). ^{1}H NMR (400 MHz, $CDCl_3$) δ 10.55 (1H, s, NC*H*N), 7.29 (2H, d, NC*HCH*N), 4.35 (4H, t, $NCH_2C_5H_{11}$), 1.92 (4H, q, $NCH_2CH_2C_4H_9$), 1.35–1.28 (12H, m, $N(CH_2)_2C_3H_6CH_3$), 0.86 (6H, t, $N(CH_2)_5CH_3$); ^{13}C NMR (75 MHz, $CDCl_3$) δ 137.10 (NH*C*N), 122.13 (NH*CC*HN), 50.09 (NCH_2), 31.09, 30.29, 25.88, 22.38, 13.90 (CH_3).

4.1.3 Syntheses of (benz)imidazolium haloaurates. Typically, 400 mg of (benz)imidazolium bromide (1 eq.) were dissolved in 20 mL of chloroform and mixed with 1 equivalent of $HAuCl_4{\cdot}3H_2O$ in water (5 mL). After 3 h of stirring at room temperature the organic phase was decanted and filtered, the solvent was evaporated and the product was dried under vacuum for a few hours, then used without further purification.

1-AuX$_4$. ^{1}H NMR (400 MHz, CD_2Cl_2) δ 8.71 (1H, s, NC*H*N), 7.35 (2H, d, NC*HCH*N), 4.25 (4H, t, $NCH_2C_{11}H_{23}$), 1.94 (4H, q, $NCH_2CH_2C_{10}H_{21}$), 1.37–1.29 (36H, m, $N(CH_2)_2C_9H_{18}CH_3$), 0.90 (6H, t, $N(CH_2)_{11}CH_3$); ^{13}C NMR (75 MHz, $CDCl_3$) δ 135.19 (NH*C*N), 122.59 (NH*CC*HN), 50.94 (NCH_2), 32.05, 30.29, 29.75, 29.65, 29.52, 29.49, 29.10, 26.48, 22.83, 14.27 (CH_3).

2-AuX$_4$. ^{1}H NMR (400 MHz, $CDCl_3$) δ 9.55 (1H, s, NC*H*N), 7.77 (4H, m, C_6H_4), 4.57 (4H, t, $NCH_2C_{11}H_{23}$), 2.09 (4H, q, $NCH_2CH_2C_{10}H_{21}$), 1.47–1.38 (36H, m, $N(CH_2)_2C_9H_{18}CH_3$), 0.90 (6H, t, $N(CH_2)_{11}CH_3$); ^{13}C NMR (75 MHz, $CDCl_3$) δ 140.33 (NH*C*N), 131.56, 127.85, 113.52, 48.34 (NCH_2), 32.04, 29.74, 29.65, 29.59, 29.54, 29.47, 29.16, 26.81, 22.82, 14.26 (CH_3).

3-AuX$_4$. ^{1}H NMR (400 MHz, $CDCl_3$) δ 8.98 (1H, s, NC*H*N), 7.28 (2H, d, NC*HCH*N), 4.29 (4H, t, $NCH_2C_5H_{11}$), 1.94 (4H, q, $NCH_2CH_2C_4H_9$), 1.35–1.29 (12H, m, $N(CH_2)_2C_3H_6CH_3$), 0.90 (6H, t, $N(CH_2)_5CH_3$); ^{13}C NMR (75 MHz, $CDCl_3$) δ 134.94 (NH*C*N), 122.77 (NH*CC*HN), 50.80 (NCH_2), 31.22, 31.13, 30.22, 30.09, 26.06, 22.49, 14.06 (CH_3).

4.1.4 Syntheses of gold nanoparticles. In a typical NaH free synthesis of Au nanoparticles, the (benz)imidazolium haloaurate (0.05 mmol) was dissolved in a toluene/dichloromethane mixture (10 mL, v/v = 1 : 1) and thermalized for 5–10 min. 10 eq. of $NaBH_4$ were dissolved separately in ~3 ml of water and added dropwise to the gold precursor, causing a discoloration of the solution before a drastic color change to deep red, which reflected the formation of gold nanoparticles. After 10 min of stirring, the mixture was rinsed with ~25 mL of water to remove any remaining salts. The nanoparticles, dispersed in the organic layer, were precipitated with ~50 mL of ethanol and centrifuged (10 733 RCF for 30 min). Two more redispersion/precipitation cycles, with 3 mL of toluene and 50 mL of ethanol, were achieved before dispersing the nanoparticles in a small amount of toluene for storage, in order to ensure optimal redispersibility.

For syntheses carried out with NaH (60% in oil), this reactant (NaH/(benz)imid ~1.5) was first dispersed in toluene (5 mL) and added dropwise to a solution of the haloaurate salt in toluene at 0 °C (10 mL), causing discoloration of the initially orange solution. The mixture was stirred for 10–15 min before adding $NaBH_4$ (~10 eq.) freshly dissolved in water (3 mL). The so-obtained gold nanoparticles were purified as in the NaH free protocol.

For syntheses with tBuNH$_2$BH$_3$, the (benz)imidazolium haloaurate (0.05 mmol) and the (benz)imidazolium bromide, when necessary, were dissolved in toluene (10 mL). The reducing agent (~10 eq.) was separately dissolved in toluene (5 mL) and both solutions thermalized for 5 min. tBuNH$_2$BH$_3$ was added dropwise and the mixture was stirred for 10 min before precipitating the Au nanoparticles in ethanol and resuspension in toluene for TEM analyses.

For syntheses with AuCl, the (benz)imidazolium bromide was dissolved in toluene and added to a toluene solution of AuCl, causing an immediate color change of the solution from colorless to orange. After approx. 10 min, a fresh aqueous solution of $NaBH_4$ (~10 eq.) was added into an ice bath, instantly producing a deep red solution, and was allowed to react for another 15 min. The precipitation of the gold nanoparticles was carried out as for the previous syntheses.

4.2. Characterization techniques

4.2.1 Transmission electron microscopy (TEM) measurements. The samples were prepared by dropping colloidal suspensions onto a copper grid coated with a carbon film, and allowing the solvent to evaporate in air. The TEM images were obtained from a Tecnai Spirit G2 microscope operating at 120 kV. Size distribution histograms were obtained by measuring at least 500 particles per sample using the ImageJ software.

4.2.2 X-ray crystal structure determination‡. Crystals suitable for X-ray crystallography were directly obtained from the slow diffusion of EtOH into $CHCl_3$ solutions of the complexes. A single crystal of the compounds was selected promptly, mounted onto a cryoloop, and transferred into a cold nitrogen gas stream. The intensity data were collected with a Bruker Kappa-APEX II with graphite-monochromated Mo-Kα radiation

(λ = 0.71073 Å). Data collection was performed with the APEX2 suite (Bruker). Unit-cell parameters refinement, integration and data reduction were carried out with the SAINT program (Bruker). SADABS (Bruker) was used for scaling and multi-scan absorption corrections. In the WinGX suite of programs,[36] the structure were solved with the SUPERFLIP[37] program and refined by full-matrix least-squares methods using SHELXL-14.[38]

4.2.3 Spectroscopic measurements. UV-Vis absorption spectra were recorded with an Agilent 8453 UV-Vis spectrophotometer. The solutions were prepared by appropriate dilution of stock solutions (*ca.* 10^{-5} M), transferred into a closed quartz cuvette, and the spectra were recorded in the 250–800 nm range with 1 nm step. ATR-FTIR (attenuated total reflectance Fourier transform infrared) spectra were recorded on a PerkinElmer spectrum 400 instrument in the 550–4000 cm^{-1} range with a 2 cm^{-1} resolution.

4.2.4 X-ray photoelectron spectroscopy (XPS). Spectra were recorded with a Thermo ESCALAB 250 X-ray photoelectron spectrometer with a monochromatic Al-K_α X-Ray source ($h\nu$ = 1486.6 eV) operating at 10^{-10} Torr. The analyzer pass energy was 50 eV for the survey spectra and 20 eV for the high-resolution spectra. All spectra were calibrated *versus* the binding energy (BE) of hydrocarbons (C 1s at 285.0 eV). Spectra were recorded and analyzed using the Thermo Avantage software. For curve fitting and decomposition, a Shirley-type background subtraction has been used and the shape of fitting curves was obtained by a 70% Gaussian/30% Lorentzian distribution.

4.2.5 Nuclear magnetic resonance (NMR) spectroscopy. ^{1}H NMR and ^{13}C NMR spectra were recorded at room temperature on a Bruker Avance 300 or Avance 400 spectrometer. Shifts (δ) are given in parts per million (ppm) using the resonance of the solvent peak as a secondary reference ($\delta(^{1}H)$ = 7.26 ppm and $\delta(^{13}C)$ = 77.16 ppm for $CDCl_3$ and $\delta(^{1}H)$ = 5.32 ppm for CD_2Cl_2). Multiplicities are reported using the following abbreviations: s (singlet), d (doublet), t (triplet), q (quartet), m (multiplet).

4.2.6 Mass spectrometry (MS). High resolution mass spectra were obtained using a mass spectrometer MicroTOF from Bruker with an electron spray ion source (ESI) and a TOF detector.

Conflicts of interest

There are no conflicts of interest to declare.

Acknowledgements

The authors acknowledge Denis Lesage for mass spectrometry measurements and Lise-Marie Chamoreau for solving the XRD crystal structures. This work was supported by the LabEx MiChem and the Labex MATISSE, both parts of French state funds managed by the ANR within the Investissements d'Avenir programme under reference ANR-11-IDEX-0004-02.

Notes and references

1 D. Astruc, F. Lu and J. R. Aranzaes, *Angew. Chem., Int. Ed.*, 2005, **44**, 7852.
2 G. A. Somorjai, A. M. Contreras, M. Montano and R. M. Rioux, *Proc. Natl. Acad. Sci. U. S. A.*, 2006, **103**, 10577.
3 (*a*) M. C. Daniel and D. Astruc, *Chem. Rev.*, 2004, **104**, 293; (*b*) C. Goldmann, R. Lazzari, X. Paquez, C. Boissiere, F. Ribot, C. Sanchez, C. Chaneac and D. Portehault, *ACS Nano*, 2015, **9**, 7572; (*c*) C. Goldmann, F. Ribot, L. F. Peiretti, P. Quaino, F. Tielens, C. Sanchez, C. Chaneac and D. Portehault, *Small*, 2017, **13**, 1604028.
4 J. M. Pettibone and J. W. Hudgens, *ACS Nano*, 2011, **5**, 2989.
5 G. Frens, *Nature, Phys. Sci.*, 1973, **241**, 20.
6 B. L. Cushing, V. L. Kolesnichenko and C. J. O'Connor, *Chem. Rev.*, 2004, **104**, 3893.
7 S. Guo and E. Wang, *Anal. Chim. Acta*, 2007, **598**, 181.
8 K. Esumi, N. Takei and T. Yoshimura, *Colloids Surf., B*, 2003, **32**, 117.
9 Z. M. Qi, H. S. Zhou, N. Matsuda, I. Honma, K. Shimada, A. Takatsu and K. Kato, *J. Phys. Chem. B*, 2004, **108**, 7006.
10 (*a*) A. V. Zhukhovitskiy, M. J. MacLeod and J. A. Johnson, *Chem. Rev.*, 2015, **115**, 11503; (*b*) K. Chang, J. G. Chen, Q. Lu and M.-J. Cheng, *J. Phys. Chem. A*, 2017, **121**, 2674; (*c*) H. Hakkinen, *Nat. Chem.*, 2012, **4**, 443; (*d*) C. M. Crudden, J. H. Horton, I. I. Ebralidze, O. V. Zenkina, A. B. McLean, B. Drevniok, Z. She, H.-B. Kraatz, N. J. Mosey, T. Seki, E. C. Keske, J. D. Leake, A. Rousina-Webb and G. Wu, *Nat. Chem.*, 2014, **6**, 409; (*e*) G. Wang, A. Rühling, S. Amirjalayer, M. Knor, J. B. Ernst, C. Richter, H.-J. Gao, A. Timmer, H.-Y. Gao, N. L. Doltsinis, F. Glorius and H. Fuchs, *Nat. Chem.*, 2017, **9**, 152; (*f*) C. M. Crudden, J. H. Horton, M. R. Narouz, Z. Li, C. A. Smith, K. Munro, C. J. Baddeley, C. R. Larrea, B. Drevniok, B. Thanabalasingam, A. B. McLean, O. V. Zenkina, I. I. Ebralidze, Z. She, H.-B. Kraatz, N. J. Mosey, L. N. Saunders and A. Yagi, *Nat. Commun.*, 2016, **7**, 12654; (*g*) C. R. Larrea, C. J. Baddeley, M. R. Narouz, N. J. Mosey, J. H. Horton and C. M. Crudden, *ChemPhysChem*, 2017, **18**, 3536.
11 (*a*) E. C. Hurst, K. Wilson, I. J. S. Fairlamb and V. Chechik, *New J. Chem.*, 2009, **33**, 1837; (*b*) M. Rodriguez-Castillo, D. Laurencin, F. Tielens, A. van der Lee, S. Clement, Y. Guari and S. Richeter, *Dalton Trans.*, 2014, **43**, 5978; (*c*) C. Richter, K. Schaepe, F. Glorius and B. J. Ravoo, *Chem. Commun.*, 2014, **50**, 3204; (*d*) A. Ferry, K. Schaepe, P. Tegeder, C. Richter, K. M. Chepiga, B. J. Ravoo and F. Glorius, *ACS Catal.*, 2015, **5**, 5414; (*e*) Z. Cao, D. Kim, D. C. Hong, Y. Yu, J. Xu, S. Lin, X. D. Wen, E. M. Nichols, K. Jeong, J. A. Reimer, P. D. Yang and C. J. Chang, *J. Am. Chem. Soc.*, 2016, **138**, 8120; (*f*) M. Rodriguez-Castillo, G. Lugo-Preciado, D. Laurencin, F. Tielens, A. van der Lee, S. Clement, Y. Guari, J. M. Lopez-de-Luzuriaga, M. Monge, F. Remacle and S. Richeter, *Chem. – Eur. J.*, 2016, **22**, 10446.

12 (*a*) J. Vignolle and T. D. Tilley, *Chem. Commun.*, 2009, 7230; (*b*) X. Ling, N. Schaeffer, S. Roland and M.-P. Pileni, *Langmuir*, 2013, **29**, 12647; (*c*) M. M. Nigra, A. J. Yeh, A. Okrut, A. G. DiPasquale, S. W. Yeh, A. Solovyov and A. Katz, *Dalton Trans.*, 2013, **42**, 12762; (*d*) S. G. Song, C. Satheeshkumar, J. Park, J. Ahn, T. Premkumar, Y. Lee and C. Song, *Macromolecules*, 2014, **47**, 6566; (*e*) M. J. MacLeod and J. A. Johnson, *J. Am. Chem. Soc.*, 2015, **137**, 7974; (*f*) K. Salorinne, R. W. Y. Man, C.-H. Li, M. Taki, M. Nambo and C. M. Crudden, *Angew. Chem., Int. Ed.*, 2017, **129**, 6294; (*g*) R. W. Y. Man, C.-H. Li, M. W. A. MacLean, O. V. Zenkina, M. T. Zamora, L. N. Saunders, A. Rousina-Webb, M. Nambo and C. M. Crudden, *J. Am. Chem. Soc.*, 2018, **140**, 1576; (*h*) M. R. Narouz, C.-H. Li, A. Nazemi and C. M. Crudden, *Langmuir*, 2017, **33**, 14211.

13 (*a*) C. J. Serpell, J. Cookson, A. L. Thompson, C. M. Brown and P. D. Beer, *Dalton Trans.*, 2013, **42**, 1385; (*b*) X. Ling, S. Roland and M.-P. Pileni, *Chem. Mater.*, 2015, **27**, 414; (*c*) S. Roland, X. Ling and M. P. Pileni, *Langmuir*, 2016, **32**, 7683.

14 J. Crespo, Y. Guari, A. Ibarra, J. Larionova, T. Lasanta, D. Laurencin, J. M. Lopez-de-Luzuriaga, M. Monge, M. E. Olmos and S. Richeter, *Dalton Trans.*, 2014, **43**, 15713.

15 (*a*) C. M. Crudden and D. P. Allen, *Coord. Chem. Rev.*, 2004, **248**, 2247; (*b*) F. E. Hahn and M. C. Jahnke, *Angew. Chem., Int. Ed.*, 2008, **47**, 3122; (*c*) J. C. Y. Lin, R. T. W. Huang, C. S. Lee, A. Bhattacharyya, W. S. Hwang and I. J. B. Lin, *Chem. Rev.*, 2009, **109**, 3561; (*d*) M. N. Hopkinson, C. Richter, M. Schedler and F. Glorius, *Nature*, 2014, **510**, 485.

16 (*a*) G. C. Fortman and S. P. Nolan, *Chem. Soc. Rev.*, 2011, **40**, 5151; (*b*) F. Glorius, in *N-Heterocyclic Carbenes in Transition Metal Catalysis*, ed F. Glorius, Springer-Verlag, Berlin Heildelberg, 2007, vol. 21, pp. 1–20; (*c*) E. Peris and R. H. Crabtree, *Coord. Chem. Rev.*, 2004, **248**, 2239; (*d*) G. C. Vougioukalakis and R. H. Grubbs, *Chem. Rev.*, 2010, **110**, 1746; (*e*) D. Gatineau, J. P. Goddard, V. Mouries-Mansuy and L. Fensterbank, *Isr. J. Chem.*, 2013, **53**, 892.

17 W. Liu and R. Gust, *Chem. Soc. Rev.*, 2013, **42**, 755.

18 (*a*) A. V. Zhukhovitskiy, M. G. Mavros, T. Van Voorhis and J. A. Johnson, *J. Am. Chem. Soc.*, 2013, **135**, 7418; (*b*) R. Zhong, A. C. Lindhorst, F. J. Groche and F. E. Kühn, *Chem. Rev.*, 2017, **117**, 1970.

19 S. V. Dzyuba and R. A. Bartsch, *Chem. Commun.*, 2001, 1466.

20 H. Schmidbaur and A. Schier, *Chem. Soc. Rev.*, 2012, **41**, 8212.

21 M. Hasan, I. V. Kozhevnikov, M. R. H. Siddiqui, A. Steiner and N. Winterton, *Inorg. Chem.*, 1999, **38**, 5637.

22 (*a*) N. Goubet, J. Richardi, P.-A. Albouy and M.-P. Pileni, *Adv. Funct. Mater.*, 2011, **21**, 2693; (*b*) X. H. Ji, X. N. Song, J. Li, Y. B. Bai, W. S. Yang and X. G. Peng, *J. Am. Chem. Soc.*, 2007, **129**, 13939.

23 W. Haiss, N. T. K. Thanh, J. Aveyard and D. G. Fernig, *Anal. Chem.*, 2007, **79**, 4215.

24 (*a*) R. W. Alder, P. R. Allen and S. J. Williams, *J. Chem. Soc., Chem. Commun.*, 1995, 1267; (*b*) R. W. Taft and F. G. Bordwell, *Acc. Chem. Res.*, 1988, **21**, 463.

25 (*a*) P. Lara, O. Rivada-Wheelaghan, S. Conejero, R. Poteau, K. Philippot and B. Chaudret, *Angew. Chem., Int. Ed.*, 2011, **50**, 12080; (*b*) E. A. Baquero, S. Tricard, J. C. Flores, E. de Jesus and B. Chaudret, *Angew. Chem., Int. Ed.*, 2014, **53**, 13220.

26 N. A. Abood, M. A. L. Askari and B. A. Saeed, *Basrah J. Sci. C*, 2012, **30**, 119.

27 L. M. Martínez-Prieto, I. Cano, A. Márquez, E. A. Baquero, S. Tricard, L. Cusinato, I. del Rosal, R. Poteau, Y. Coppel, K. Philippot, B. Chaudret, J. Cámpora and P. W. N. M. van Leeuwen, *Chem. Sci.*, 2017, **8**, 2931.

28 A. Rühling, K. Schaepe, L. Rakers, B. Vonhören, P. Tegeder, B. J. Ravoo and F. Glorius, *Angew. Chem., Int. Ed.*, 2016, **55**, 5856.

29 H. K. Kim, A. S. Hyla, P. Winget, H. Li, C. M. Wyss, A. J. Jordan, F. A. Larrain, J. P. Sadighi, C. Fuentes-Hernandez, B. Kippelen, J.-L. Bredas, S. Barlow and S. R. Marder, *Chem. Mater.*, 2017, **29**, 3403.

30 (*a*) D. Mercier, N. Leconte, C. Methivier, F. Suzenet, G. Guillaumet, A. Wuillaume and C.-M. Pradier, *Phys. Chem. Chem. Phys.*, 2010, **12**, 6099; (*b*) V. Lockett, R. Sedev, C. Bassell and J. Ralston, *Phys. Chem. Chem. Phys.*, 2008, **10**, 1330.

31 A. Batra, G. Kladnik, N. Gorjizadeh, J. Meisner, M. Steigerwald, C. Nuckolls, S. Y. Quek, D. Cvetko, A. Morgante and L. Venkataraman, *J. Am. Chem. Soc.*, 2014, **136**, 12556.

32 K. Boukerma, M. M. Chehimi, J. Pinson and C. Blomfield, *Langmuir*, 2003, **19**, 6333.

33 F. Petraki, V. Papaefthimiou and S. Kennou, *Org. Electron.*, 2007, **8**, 522.

34 S. Gardner, T. Kawamoto and D. P. Curran, *J. Org. Chem.*, 2015, **80**, 9794.

35 M. P. Rowe, K. E. Plass, K. Kim, C. Kurdak, E. T. Zellers and A. J. Matzger, *Chem. Mater.*, 2004, **16**, 3513.

36 L. J. Farrugia, *J. Appl. Crystallogr.*, 1999, **32**, 837.

37 L. Palatinus and G. Chapuis, *J. Appl. Crystallogr.*, 2007, **40**, 786.

38 G. M. Sheldrick, *Acta Crystallogr., Sect. C: Struct. Chem.*, 2015, **71**, 3.